Please cite this article in press as: Ribeiro et al., The Structure and Regulation of Human Muscle α-Actinin, Cell (2014), http://dx.doi.org/10.1016/j.cell.2014.10.056

The Structure and Regulation of Human Muscle α-Actinin

Euripedes de Almeida Ribeiro, Jr.,[1,10] Nikos Pinotsis,[1,10] Andrea Ghisleni,[2,10] Anita Salmazo,[1] Petr V. Konarev,[3] Julius Kostan,[1] Björn Sjöblom,[1] Claudia Schreiner,[1] Anton A. Polyansky,[1,8] Eirini A. Gkougkoulia,[1] Mark R. Holt,[2] Finn L. Aachmann,[4] Bojan Žagrović,[1] Enrica Bordignon,[5,9] Katharina F. Pirker,[6] Dmitri I. Svergun,[3] Mathias Gautel,[2,*] and Kristina Djinović-Carugo[1,7,*]

[1]Department of Structural and Computational Biology, Max F. Perutz Laboratories, University of Vienna, Campus Vienna Biocenter 5, 1030 Vienna, Austria

[2]British Heart Foundation Centre of Research Excellence, Randall Division for Cell and Molecular Biophysics and Cardiovascular Division, King's College London, London SE1 1UL, UK

[3]European Molecular Biology Laboratory, Deutsches Elektronen-Synchrotron, Notkestrasse 85, 22603 Hamburg, Germany

[4]Department of Biotechnology, Norwegian University of Science and Technology, Sem Sælands vei 6/8, 7491 Trondheim, Norway

[5]Laboratory of Physical Chemistry, ETH Zurich, Vladimir-Prelog-Weg 2, 8093 Zurich, Switzerland

[6]Division of Biochemistry, Department of Chemistry, University of Natural Resources and Life Sciences, Muthgasse 18, 1190 Vienna, Austria

[7]Department of Biochemistry, Faculty of Chemistry and Chemical Technology, University of Ljubljana, Aškerčeva 5, 1000 Ljubljana, Slovenia

[8]M.M. Shemyakin and Yu.A. Ovchinnikov Institute of Bioorganic Chemistry, Russian Academy of Sciences, Moscow 117997, Russia

[9]Fachbereich Physik, Freie Universität Berlin, Arnimallee 14, 14195 Berlin, Germany

[10]Co-first author

*Correspondence: mathias.gautel@kcl.ac.uk (M.G.), kristina.djinovic@univie.ac.at (K.D.-C.)

http://dx.doi.org/10.1016/j.cell.2014.10.056

SUMMARY

The spectrin superfamily of proteins plays key roles in assembling the actin cytoskeleton in various cell types, crosslinks actin filaments, and acts as scaffolds for the assembly of large protein complexes involved in structural integrity and mechanosensation, as well as cell signaling. α-actinins in particular are the major actin crosslinkers in muscle Z-disks, focal adhesions, and actin stress fibers. We report a complete high-resolution structure of the 200 kDa α-actinin-2 dimer from striated muscle and explore its functional implications on the biochemical and cellular level. The structure provides insight into the phosphoinositide-based mechanism controlling its interaction with sarcomeric proteins such as titin, lays a foundation for studying the impact of pathogenic mutations at molecular resolution, and is likely to be broadly relevant for the regulation of spectrin-like proteins.

INTRODUCTION

Mobility is essential to all living organisms, from organelle transport to movement of entire organisms. In many motile systems, actin and myosin filaments assume ordered arrays organized by specific actin or myosin ligands. In higher animals, movement is performed by striated muscle, defined by highly regular arrangements of visible striations. The minimal contractile unit of striated muscle is the sarcomere, which is anchored and stabilized by transverse crosslinking structures at the two lateral Z-disk boundaries, the A-band and the central M-band (Gautel, 2011; Tskhovrebova and Trinick, 2010). In vertebrates, the giant protein titin (connectin) spans Z-disks to M-bands and may act as a blueprint for sarcomere assembly (Gautel, 2011; Tskhovrebova and Trinick, 2010). Within the vertebrate Z-disk, a complicated network of protein-protein interactions anchors and stabilizes the actin and the elastic titin filaments (Luther, 2009).

α-actinin was originally described as an actin-crosslinking Z-disk protein in muscle (Masaki et al., 1967), but its four closely related isogenes (*ACTN1–4*) fulfil similar functions in all cell types (Foley and Young, 2014; Sjöblom et al., 2008). α-actinin, in particular isoform 2 (encoded by *ACTN2*), is the major Z-disk component, where it plays a central role crosslinking actin and titin filaments. α-actinin is an antiparallel homodimer of more than 200 kDa, comprising an N-terminal actin-binding domain (ABD), a central domain of four spectrin-like repeats (SRs), and a C-terminal calmodulin-like domain (CAMD) with two pairs of EF hand motifs (EFs) (Figure 1A). Because the SR region appears to have a cylindrical shape, it is also called the rod domain.

The elementary structure of the Z-disk is that of a tetragonal array of antiparallel actin filaments spaced 240 Å apart and crosslinked by successive layers of filaments at intervals of ≈190 Å rotated by 90° between each layer along the myofibril axis (Goldstein et al., 1979). These filaments correlate with α-actinin crosslinks, but the molecular layout of α-actinin that allows strict alternating crosslinks between actin filaments remains elusive (reviewed in Luther, 2009).

In striated muscle, α-actinin also binds differentially spliced titin Z-repeats, possibly regulating the number of crosslinking α-actinin molecules (Gautel et al., 1996). These titin Z-repeats contain a short, hydrophobic α-actinin-binding motif, which interacts with the CAMD (Atkinson et al., 2001; Sorimachi et al., 1997; Young et al., 1998). Additionally, α-actinin binds a plethora

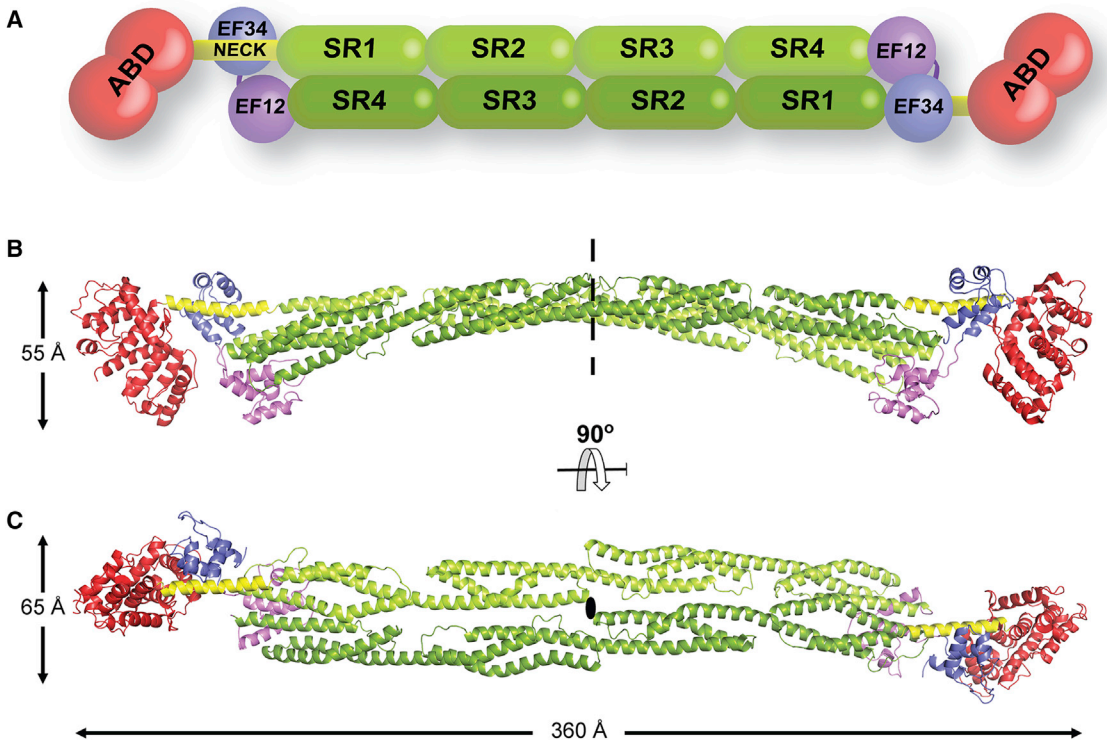

Figure 1. Complete Structure of α-Actinin-2 in Closed Conformation

(A) Domain composition of the α-actinin dimer. Color code, as in all the following figures: ABD, red; neck, yellow; SR1–SR4, green; EF1-2, violet; EF3-4, blue.

(B) The dimeric structure of α-actinin-2 assembled from two halves of the α-actinin-2 protomer (ABD-SR1-SR2/SR3-SR4-CaM) through a crystallographic 2-fold axis (dashed line; ellipse in C). Overall dimensions are indicated.

(C) Same as in (B), rotated 90° around the horizontal axis.

See also Table S1.

of cytoplasmic and membrane proteins in striated muscle and nonmuscle tissues (Djinovic-Carugo et al., 2002; Foley and Young, 2014). To achieve ordered cytoskeletal assemblies, the binding properties of α-actinin must be spatiotemporally regulated. Actin binding of nonmuscle isoforms is regulated by binding of Ca^{2+} ions to the CAMD (Foley and Young, 2014). In contrast, muscle α-actinin is calcium insensitive, and its F-actin- and titin-binding properties are likely regulated by phospholipids (most notably phosphatidylinositol bisphosphate; PIP2) (Fukami et al., 1992; Young et al., 1998; Young and Gautel, 2000). Despite being a major integrator of titin and actin in one of the stiffest structures of the sarcomere, muscle α-actinin shows surprisingly dynamic association with the Z-disk actin cytoskeleton (Sanger and Sanger, 2008), suggesting that its actin and titin binding activity must be dynamically regulated.

Biochemical analysis led us to propose previously that the α-actinin-titin interaction is regulated by an intramolecular mechanism where a short sequence in α-actinin between the ABD and the rod interacts with the CAMD in a pseudoligand mechanism (Young and Gautel, 2000). A similar mode of interaction has been found for the α-actinin ligand palladin (Beck et al., 2011).

Here, we report the crystal structure of human α-actinin-2 at 3.5 Å resolution. It is a complete high-resolution α-actinin-2 structure, revealing insight into the mechanism that promotes the molecular assembly of the Z-disk and the intramolecular contacts that regulate these interactions. Furthermore, the structure provides a template for the α-actinin and spectrin superfamily and insight into the impact of disease-associated genetic variants in ACTN genes.

RESULTS

Closed Structure of α-Actinin-2

Overall Architecture

The structure of α-actinin-2 was solved and refined to 3.5 Å resolution to an R_{work}/R_{free} of 20.5%/25.8% (Table S1 available online). The α-actinin-2 dimer reveals a cylindrical shape ~360 Å long and ~60 Å wide (Figures 1B and 1C). Each protomer comprises an N-terminal ABD followed by an α-helical linker (neck), four spectrin-like repeats (SR1–4), and a C-terminal CAMD of two pairs of EF hands (EF1-2 and EF3-4). The first 34 and last 2 residues are missing from our model. Two antiparallel SR1–4s that assemble the core of the extended structure form the central portion of the dimer (rod). The two ABDs and two CAMDs flank the elongated assembly at its ends.

As expected, in the absence of actin, the ABD is in a closed conformation, in which the two calponin homology domains (CH1 and CH2) are in extensive contact, similar to the

arrangement found in α-actinin-3, plectin, and fimbrin ABD domains (Franzot et al., 2005; Klein et al., 2004).

The ABD is linked to the first spectrin-like repeat (SR1) of the rod through the six-turn α-helical neck that is flanked by two hinges, the first on residue G258 linking the ABD to the neck and the second on residue M283 linking the neck to SR1 (Figure 2A).

Comparison of the spectrin-like repeats in the full-length α-actinin-2 structure with the previously determined dimeric rod domain (Ylänne et al., 2001) (Protein Data Bank [PDB] ID code 1HCI) reveals high similarity between SR2, SR3, and SR4 and minor differences for SR1 (Table S2). However, although the α helices of the two SR4 domains are well aligned, there are large deviations between α helices h1 and h2 due to contacts of EF1-2 positioned over this loop in the full-length structure (Figures 1 and 2B; Figure S1A). The antiparallel α-actinin-2 dimer assembles predominately via the rod domain. The two ABDs are flanked at both termini along the long axis of the rod and are stabilized in their position by a few polar interactions with the neck region and EF3-4.

The C-terminal CAMD is divided into structurally distinct N- and C-terminal lobes: EF hands 1-2 and 3-4 connected by a short linker. The overall structure of each lobe is well defined through the main-chain atoms on the α helices of the EF hands. As expected, no density conforming to bound calcium was detected, and the architecture of the CAMD resembles calcium-free conformations of calmodulin (see below).

Calmodulin-like Domain Conformation and Interactions

The EF3-4 accommodates the α helix of the neck from the juxtaposed α-actinin-2 protomer through its hydrophobic cleft. This classifies the EF3-4-neck interaction as 1:1 or canonical (Hoeflich and Ikura, 2002), involving the cavity formed by the first helix of the EF3-4, the linker between the EF3-4 helices, and the C-terminal helix of the lobe (Figures 2C and 2D). The EF3-4-neck interface is mainly hydrophobic, supported with a few H-bonds (Figure 2C). The neck region displays the known hydrophobic Ca^{2+}/calmodulin (CaM)-binding motif, termed 1-4-5-8 (Bayley et al., 1996), with hydrophobic A266, I269, C270, and L273 at these positions (Figure 2F). Additionally, EF3-4 interact with the connecting loop of α helices 2 and 3 from SR1 via an H-bond and a π-stacking interaction, supporting previous reports that SR1 stabilizes the interaction with EF3-4 (Young and Gautel, 2000). The overall binding interface of EF3-4 is ~500 $Å^2$, representing 11% of its total surface area. The root-mean-square deviation (rmsd) with the C-terminal lobe in complex with Zr-7 of titin (Atkinson et al., 2001) (PDB ID code 1H8B) is 1.1 Å for 64 equivalent Cα atoms, implying no significant conformational difference.

EF1-2 are less well defined in the electron density compared to the C-terminal lobe, and similar to EF3-4 show a binding interface of ~500 $Å^2$ with SR4. The interactions occur between the N-terminal α helix of EF1-2, the loop connecting EF1 and EF2 intercalates between α helices 2 and 3 of SR4, whereas the C-terminal α helix of EF1-2 lies in a parallel orientation on the third α helix 3 of SR4 (Figure 2B). In essence, only the N- and C-terminal helices of EF1-2 are involved in the binding, and this mode has no resemblance to any known classification of calmodulin-like domains but rather is similar to a bound-free lobe (Hoeflich and Ikura, 2002).

Interestingly, even though EF1-2 and EF3-4 have different interaction interfaces, they both adopt the same semiopen conformation (Chin and Means, 2000; Swindells and Ikura, 1996) (Figure S1B). The interaction of EF3-4 with the neck resembles that with titin Zr-7, both in terms of domain structure and ligand binding (Atkinson et al., 2001) (Figure 2F). EF1-2 and EF3-4 are mostly similar to the C-terminal lobe of human cardiac troponin C (TnC) (rmsd 3.1 and 3.2 Å for EF1-2 and EF3-4, respectively, with the C-terminal TnC lobe; PDB ID code 1J1E) (Takeda et al., 2003), confirming a previous observation that side-chain clusters in the EF hands are not related to the semiopen conformation (Atkinson et al., 2001). Further details on CAMD conformation can be found in Supplemental Information.

Sequence alignment of the EF hand pairs from α-actinin-2 and TnC reveals that in α-actinin-2, several calcium ligands in TnC, typically D, N, and E, are replaced by bulkier charged or smaller residues (Figure 2E). In essence, an R inhibits calcium binding in EF1 and a longer Q in EF2, where also a smaller S occupies the last position. In EF3, two positions typically occupied by a negatively charged D host an A and a P, whereas no residue promoting calcium binding is found in EF4.

Molecular Determinants of EF3-4 Ligand Specificity

Young and Gautel (2000) showed that CAMD binds to the neck region with lower affinity than to Zr-7 (K_d of 0.57 μM and 0.19 μM, respectively). In order to understand the higher affinity of CAMD for Zr-7, we compared the interaction interfaces of CAMD with Zr-7 (Atkinson et al., 2001) and the neck region.

Structural superposition of EF3-4 domains in complex with the ligands shows a similar layout between the α helices of the neck and Zr-7 in complex with CAMD (Figure 2F). Comparison of the 1-4-5-8 motifs shows that titin Zr-7 hosts a bulkier hydrophobic residue at position 1 (V702/A266), whereas position 5 in the neck is a less bulky Cys residue at position 270 (cf V706 in Zr-7) (Carugo, 2014), resulting in reduced stabilization of the interaction. This is reflected in the increase of the probability measure $P_{\Delta G,IF}$ for the interface derived from the gain in solvation energy upon complexation, where $P_{\Delta G,IF} > 0.5$ points to hydrophilic/unspecific and $P_{\Delta G,IF} < 0.5$ points to hydrophobic/specific interfaces using PISA (Krissinel and Henrick, 2007). Calculated for the ligand, these range from 0.31 in the EF3-4-Zr-7 complex to 0.49 for the EF3-4-neck complex, indicating a reduced specificity with a concomitant increased hydrophilic nature of the interaction.

PIP2 Binding Site

The model of α-actinin-2 and -3 activation by PIP2 hypothesizes that PIP2 docks with the polar head group on the CH2 domain, whereas its aliphatic chain reaches the CAMD binding site on the neck, perturbing this interaction (Franzot et al., 2005). This regulatory mechanism requires spatial proximity of the PIP2 binding site and neck region. The PIP2 binding site was originally mapped to residues 165–181 (Fraley et al., 2003; Fukami et al., 1996) on a loop connecting the first and second α helix of the CH2 domain. Structural analysis of the ABD of α-actinin-3 suggested a triplet of positively charged residues, which form a platform for PIP2 binding (α-actinin-2 residues R163, R169, and R192) (Franzot et al., 2005).

We used molecular dynamics (MD) simulations and flexible ligand docking to place PIP2 into the structure of α-actinin-2. Although the results suggest that the PIP2 binding site is likely

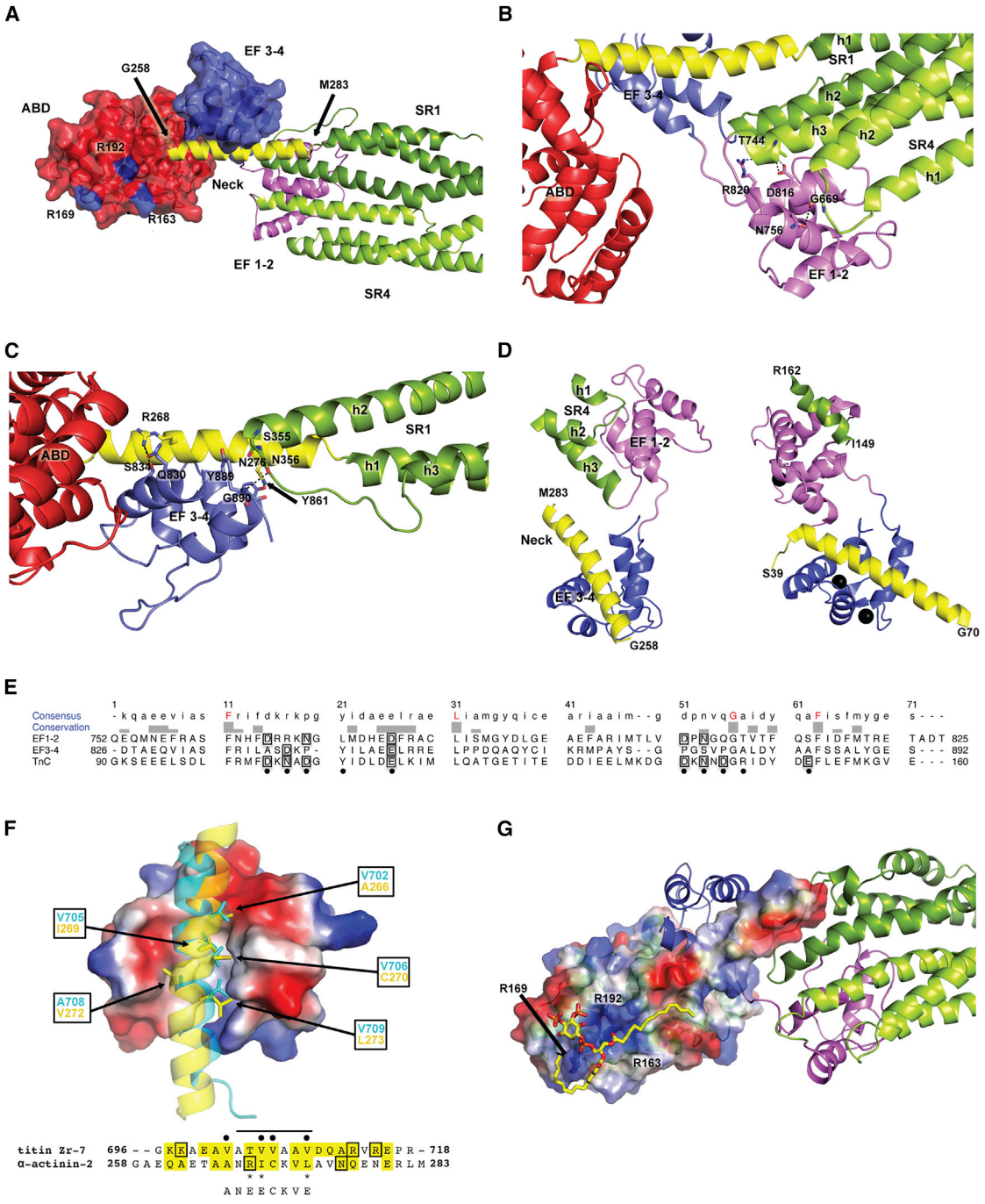

Figure 2. Close-Up of the Functional Domain Interactions

(A) PIP2 binding site on α-actinin-2 and the EF3-4-neck interaction. ABD and EF3-4 are presented with their solvent-accessible surface areas. The R residues responsible for PIP2 binding are highlighted in blue on the ABD surface.

(B) Detail of EF1-2 interactions with SR4.

(C) Detail of EF3-4 interactions with the neck region and SR1.

(D) Comparison of α-actinin-2 CAMD with TnC bound to TnI, aligned on EF3-4 and the C-terminal lobe of TnC. Left: cartoon representation of α-actinin EF1-2 and EF3-4 with the interacting portion of the neck from the juxtaposed subunit (yellow) and a part of SR4 from the same subunit. Right: cartoon representation of TnC bound to TnI. N-terminal lobe, violet, as in EF1-2, and the C-terminal lobe, blue, as in EF3-4. Bound N-terminal TnI fragment, yellow; C-terminal TnI helix, green. Calcium ions are shown as black spheres (on TnC). The C-terminal lobe of TnC is aligned to EF3-4. To show the direction of bound helices, residues defining the neck domain of actinin and TnI fragments are indicated.

(E) Sequence alignment of EF1-2 and EF3-4 and the C-terminal lobe of TnC. The corresponding calcium-binding positions in Ca^{2+}/CaM are indicated by black dots. Charged residues involved in calcium binding are boxed. Fully conserved residues are highlighted in red.

(legend continued on next page)

not rigid, a large fraction of docked poses exhibits important commonalities. Namely, in about 40% of 10,000 generated models of the complex, the polar PIP2 head directly interacts with the above-mentioned arginine platform. This was supported by fluorescence anisotropy using PIP2 binding site mutants (Figures S2A and S2B). At the same time, one (~35% of models; Figure 2G) or both (~4% of models; Figure S2F) PIP2 aliphatic chains, which span some 17 Å, lean on the partially hydrophobic surface of the ABD and extend toward the 1-4-5-8 motif in the neck region (Figure 2G). A similar binding mode, where not only the polar head is involved but also the aliphatic chain, has been observed in the matrix domain of HIV-1 (Saad et al., 2006). This suggests that the architecture of the α-actinin-2 wild-type (WT) provides a suitable spatial orientation of both PIP2 and CAMD binding sites.

Structure of Activated α-Actinin

The biochemical model suggests that α-actinin is activated by PIP2 binding to ABD, resulting in a release of EF3-4 from the neck, thus facilitating its interaction with titin (Young and Gautel, 2000).

Structure-guided mutants were designed to disrupt key contacts between the neck segment of α-actinin-2 and EF3-4, producing a constitutively open variant. In particular, one positively charged residue (R268) and two hydrophobic residues (I269, L273) were replaced by negatively charged glutamates (R268E/I269E/L273E), hereafter termed NEECK (Figure 2F). NEECK was used to validate the closed conformation observed in the crystal structure of WT α-actinin and to probe in cellula the biological relevance of the opening/closing mechanism.

Conformational Switch of α-Actinin Is Modulated by PIP2 and Titin Zr-7

We explored whether the molecular architecture observed in the crystal structure of α-actinin-2 is maintained in solution and how this is altered in NEECK as a model of the open state.

We used site-directed spin labeling and electron paramagnetic resonance (EPR) spectroscopy to obtain structural information on WT and NEECK α-actinin. All possible pairwise distances between labeled cysteines were computed (Figure 3A) and compared to those obtained by Q band double electron-electron resonance (DEER) experiments, showing a bimodal distribution peaking at 30 Å and below 20 Å (Figure 3B; Table S3). The experimental and computed distributions fit well in the distance range up to 35 Å (Figure 3B), confirming that the structures of α-actinin-2 in the crystal and solution are comparable.

We focused on the distance range below and around 20 Å, because the distance between C270 in the neck and C862 in EF3-4 is 12 ± 0.2 Å (Figure 3A). This spin label pair could sense open and closed conformations of α-actinin-2. Other spin label sites within a 20 Å distance are buried or located on the rigid rod domain (Table S3).

An open conformation of NEECK was inferred from a decreased fraction of short distances between C270 and C862 in the DEER distribution compared with WT (Figure 3C). This change in distances was validated with low-temperature continuous-wave (cw) EPR (Figures S3A and S3B).

The analysis of the crystal structure using MD/docking suggests that the PIP2 binding site on ABD maps at a suitable position and distance from the CAMD-neck interaction to sense the hydrophobic tail of PIP2 (Figures 2A and 2G; Figures S2C–S2F). Can PIP2 alone induce opening of α-actinin-2? DEER measurements were carried out on WT α-actinin-2 using the more hydrophilic PIP2 analog Bodipy-TMR-PIP2-C16 (PIP2-C16*; Figure 3C; Figures S2 and S3). No significant changes were detectable in the short distance range (Figure 3C; Figure S3).

We tested whether titin Zr-7 could act on the conformational equilibrium of α-actinin-2. We addressed this question structurally by EPR spectroscopy and quantitatively by microscale thermophoresis (MST). Addition of Zr-7 plus PIP2-C16* to α-actinin-2 significantly reduced the short distance peaks in the DEER distance distribution, indicating conversion to an open conformation. A similar effect was observed after addition of 15-fold molar excess of Zr-7 to α-actinin alone in the absence of PIP2-C16* (Figure 3C; Figures S3C and S3D). This decrease was validated by cw EPR at low temperature (Figure S3E).

The effect of PIP2-C16* on α-actinin affinity to Zr-7 was quantified by MST (Figures 3D–3F; Table S4). PIP2-C16* bound to WT α-actinin with K_d 2.96 ± 0.26 μM (Figure 3D). The results showed a significantly higher affinity of titin Zr-7 for the PIP2-C16*-α-actinin complex (Figure 3F; K_d 0.38 ± 0.06 μM) compared to α-actinin alone (K_d 2.90 ± 0.12 μM). The nanomolar Zr-7 binding affinity for the PIP2-C16*-α-actinin complex is comparable to that observed for the isolated CAMD (EF1–4) and Zr-7 (Figure 3E; K_d 0.24 ± 0.04 μM), whereas NEECK shows an intermediate affinity (Figure 3E; K_d 0.92 ± 0.02 μM) in the absence of PIP2-C16*. The results for CAMD agree with earlier binding studies (Table S4). MST thus confirms that PIP2-C16* increases Zr-7 affinity for α-actinin-2 ~10-fold, whereas the PIP2 mutant—having lower PIP2-C16* affinity (Figure 3D)—showed an insignificant increase of Zr-7 binding by PIP2-C16* (Figure 3F; Table S4).

We used small-angle X-ray scattering (SAXS), multiangle static laser light scattering (MALLS), and size-exclusion chromatography (SEC) on WT and NEECK α-actinin to understand the structural differences between closed and open conformations. The derived molecular parameters are given in Figures 4A and 4B and Table S5. SEC-MALLS shows that both α-actinin

(F) Comparison of interactions between Zr-7 and the neck α helices with EF3-4. Electrostatic surface representation of the EF hands and cartoon representation for Zr-7 (cyan) and the α-actinin-2 neck (yellow). Side chains of key hydrophobic residues are shown as sticks; sequence numbers are boxed. Structural sequence alignment between titin Zr-7 and the neck. Residues involved in the interface with EF3-4 are highlighted in yellow. Residues involved in H bonding are boxed. Asterisks denote the mutations in the NEECK mutant. Black dots denote the CaM-binding motif 1-4-5-8. Underneath is shown the sequence of the NEEK mutant. (G) α-actinin-2 with docked PIP2 (the overall top-scoring pose is shown as a yellow stick model) together with the EF3-4-neck interaction. The top-scoring pose with two PIP2 tails in contact with the neck region is presented in Figure S2F. ABD and the neck region are presented with their solvent-accessible surface areas colored by electrostatic potential and the rest by cartoon representation and color coded as in Figure 1. The three R residues responsible for PIP2 binding are indicated.

See also Table S2.

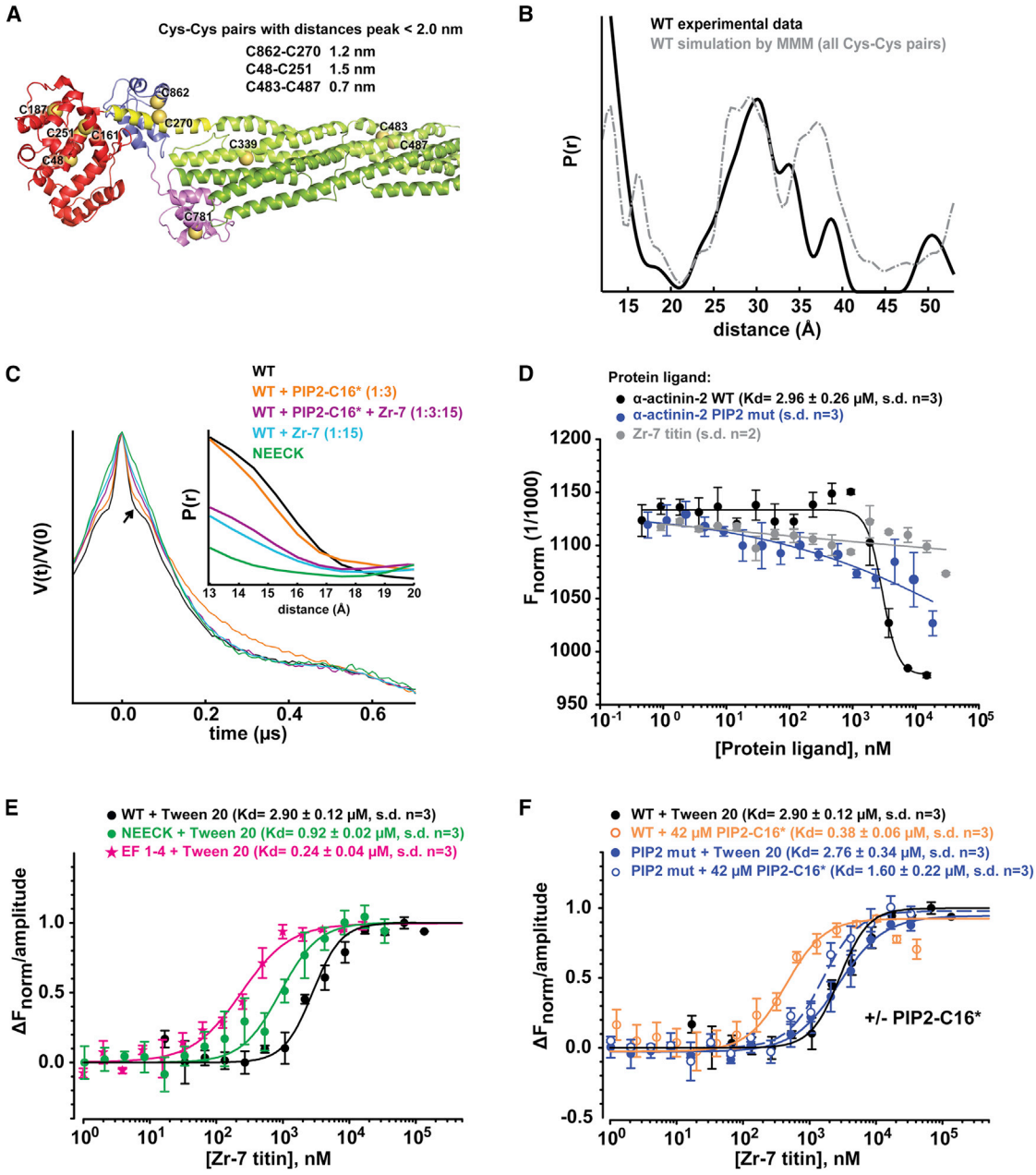

Figure 3. Structural Plasticity and Regulation of α-Actinin-2 Assessed by EPR and MST

(A) Cluster of the ten cysteine residues (Cα in dark yellow spheres) of α-actinin-2 used for the computed DEER distance distribution shown in (B). The inset shows pairs with interspin distances <20 Å.

(B) Experimental distance distribution of spin-labeled α-actinin WT (black) and simulation of the distance distribution (gray) based on spin-labeled cysteine residues from the crystal structure using the program MMM (see Extended Experimental Procedures and Table S3).

(C) DEER traces (for better comparison, adjusted by the modulation depth) and distance distributions from Q band DEER experiments using a DEER dipolar evolution time of 1 µs at 50 K of α-actinin-2 WT (black), WT plus PIP2-C16* (orange), WT plus PIP2-C16* plus Zr-7 (magenta), WT plus Zr-7 (light blue), and the NEECK mutant (green). The arrow indicates the change in the time domain trace, which is reflected in the variation of the fraction of distances <20 Å (inset).

(D) PIP2-C16* binding to α-actinin-2 measured by MST.

(E) CAMD, α-actinin-2 WT, and NEECK variant binding to Zr-7 measured by MST. The affinity determined for α-actinin-2 (+PIP2-C16*) binding to Zr-7 is in a similar range of affinity for α-actinin-2 CAMD and is implicated in Zr-7 interaction, as well as for the NEECK variant.

(F) α-actinin-2 variant binding to Zr-7 with and without PIP2-C16* measured by MST. Unlabeled Zr-7 was titrated into a fixed concentration of fluorescently labeled α-actinin-2 (50 nM).

Average and error bars (SDs) of three MST experimental replicas are plotted. Mean and SD of K_d values were calculated from these plots.

See also Tables S3 and S4.

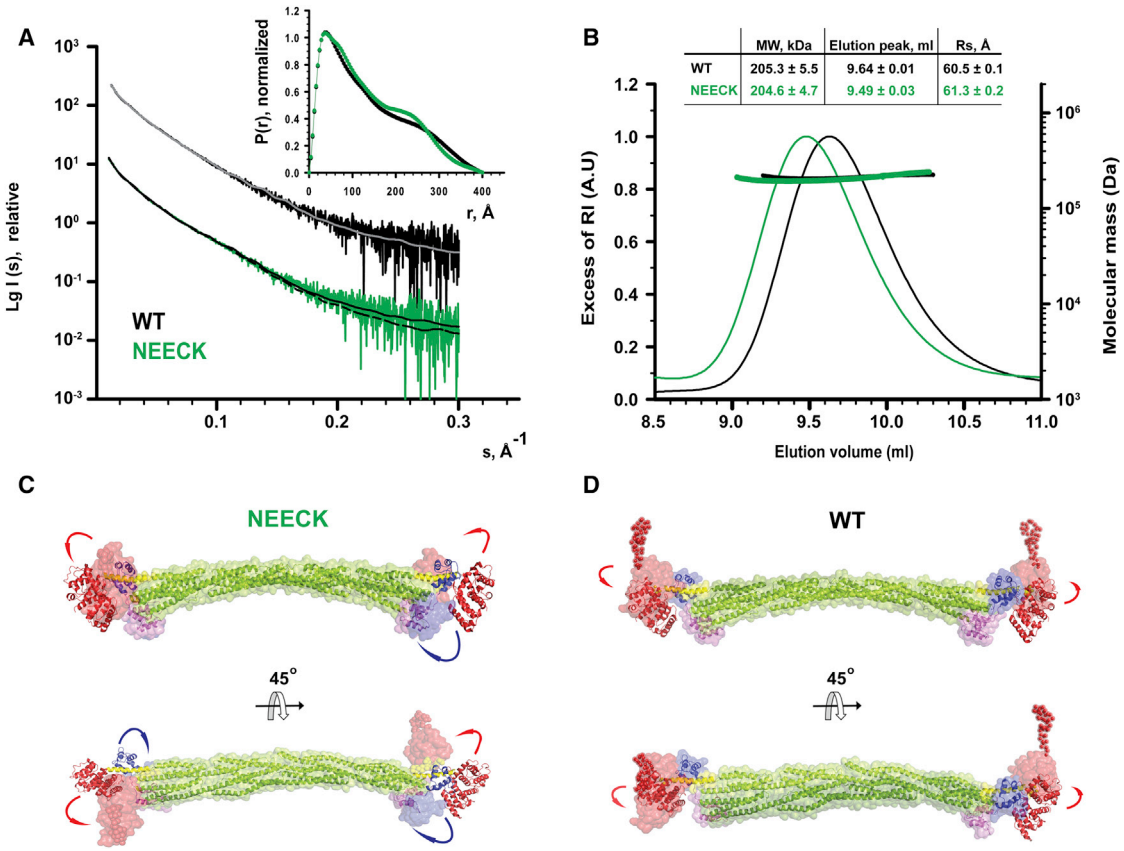

Figure 4. Solution Structure of α-Actinin-2 and the NEECK Mutant Derived from SAXS

(A) Experimental SAXS data of WT (black) and the NEECK mutant (green) of α-actinin-2. SAXS curves are computed from a rigid-body (RB) model for WT (gray) and NEECK (black). The logarithm of scattering intensity (I) is plotted as a function of the momentum transfers (s, Å^{-1}). Successive curves are displaced by one logarithmic unit for better visualization. Distance distribution functions (inset) P(r) for WT and NEECK assume slightly different shapes. RB modeling fits the experimental WT data with χ 1.25 (gray line) and experimental NEECK data with χ 1.14 (dashed black line). The fit discrepancy for NEECK increased to 1.32, assuming a helical neck (solid black line).

(B) Characterization of hydrodynamic properties of α-actinin WT and the NEECK mutant by SEC-MALLS. The lines across the protein elution volume show the molecular masses (MWs) of proteins. SEC-MALLS shows that NEECK has the same molecular weight as WT α-actinin-2 but a higher Stokes radius Rs (inset; data are represented as mean ± SD of three experiments), corroborating the open conformation for NEECK suggested by SAXS (C). AU, arbitrary units.

(C) RB model of NEECK in solvent-accessible surface representation. The neck region was modeled as a flexible linker between the rigid bodies ABD and rod, with no contact restraint. Only one RB model is shown for clarity out of three independent BUNCH runs (Figure S5A).

(D) The best RB model of WT α-actinin-2 in solvent-accessible surface representation superimposed on the crystal structure. For WT RB modeling, only ABD was allowed a variable position, whereas EF hands 3-4 were fixed in contact with the neck.

In all models, N-terminal residues missing from the crystal structure were modeled as dummy atoms. Arrows highlight the movement of ABD and EF hands 3-4 relative to the superimposed crystal structure. See also Table S5.

samples display the same molecular mass but that NEECK has an increased Stokes radius. In order to model the NEECK variant, we first addressed the structural consequences for the α-helical neck upon release of EF3-4 by performing NMR of the WT free neck peptide (amino acids A259–Y286). Analysis of 2D nuclear Overhauser effect spectroscopy (NOESY) showed no evidence of stable secondary structure (Figure S4). NEECK was thus modeled with a flexible neck region (Figure 4C), whereas the neck for WT was modeled as a rigid-body α helix, as in the X-ray structure (Figure 4D). The best WT model fits with the crystal structure (χ = 1.25). In NEECK, the ABDs deviate from the linear alignment with the rod and EF3-4 are in open conformation (Figure 4C), giving a fit of χ = 1.14. This agrees with increased mobility of NEECK and unfolding of the neck. In addition, we found a change in spin label mobility between WT and NEECK α-actinin using cw EPR room temperature measurements (Figure S5F). The narrower lines in the EPR spectrum of NEECK (Figure S5F) indicated increased mobility compared to WT, in line with an open conformation of NEECK. Thus, the solution structure of NEECK can best be modeled by an ensemble of conformations (Bernadó et al., 2007) where ABD and CAMD adopt various orientations (Figures S5A and S5E).

In conclusion, NEECK adopts a constitutively open conformation, and although it has to be seen as a "hyperactive" state, it is likely to approximate the Zr-7-bound structure of α-actinin in the Z-disk.

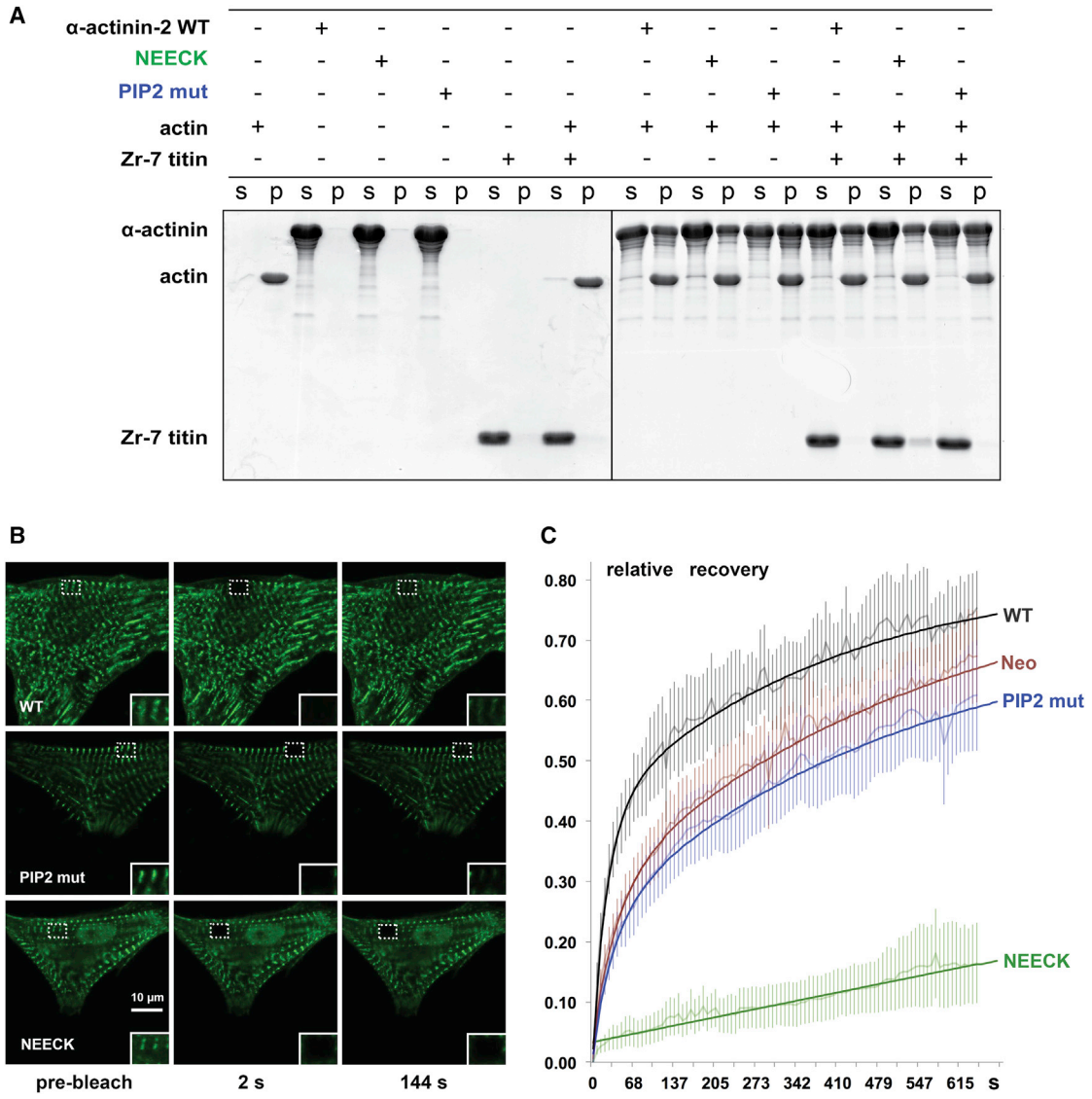

Figure 5. Mutations Affecting Regulation of α-Actinin-2 with PIP2 Do Not Influence F-Actin Binding but Impact α-Actinin-2 Z-Disk Dynamics

(A) Binding of α-actinin-2 variants to F-actin and titin Zr-7. α-actinin-2 WT, NEECK, and PIP2 mutants (PIP2 mut) were cosedimented with actin, and equal amounts of supernatant (s) and pellet (p) fractions were subjected to SDS-PAGE and visualized by Coomassie blue.

(B and C) FRAP measurements of α-actinin-2 dynamics in live NRCs expressing GFP-labeled α-actinin-2 variants (WT, PIP2 mutants, and NEECK).

(B) Snapshots at prebleach and two time points postbleach; the bleached region of interest (ROI) is highlighted by a dotted box. Note that NEECK fluorescence does not recover within the 144 s time course shown here, whereas rapid recovery is observed for WT α-actinin. Insets: ROIs enlarged 2-fold.

(C) Quantification of fluorescence intensity recovery. Note that the slowed fluorescence recovery of the PIP2 mutant is mirrored by treatment with 500 μM neomycin (Neo). Bold lines, exponential fits; shaded lines, average values. Error bars indicate SD.

Impaired α-Actinin Regulation Disrupts Coordinated Z-Disk Assembly

To directly test the role of α-actinin regulation in Z-disk assembly, we performed live-cell imaging. We hypothesized that disrupted coordination of α-actinin-2-ligand interactions in NEECK, which binds titin constitutively, and the PIP2 mutant, where activation by PIP2 is blunted, should reduce dynamic exchange of α-actinin at Z-disks.

We assessed whether the NEECK and PIP2 mutants can still play their basic roles—binding to F-actin and titin Zr-7—by actin cosedimentation assays. F-actin binding was unaffected in both mutants (Figure 5A), in contrast to PIP2-binding mutants in nonmuscle α-actinin (Fraley et al., 2003). No cosedimentation of Zr-7 was seen with WT or PIP2 mutant, in contrast to NEECK. Together, these results suggest that the PIP2 or NEECK mutations do not impair F-actin binding, and that NEECK induces PIP2-independent Zr-7 binding.

We carried out fluorescence recovery after photobleaching (FRAP) studies in neonatal rat cardiomyocytes (NRCs) expressing the GFP-labeled α-actinin-2 mutants to assess the impact of

α-actinin-2 regulation on spatiotemporal dynamics in sarcomeres. The exchange of WT α-actinin-2 at Z-disks was rapid, with a fast component $t_{1/2}$ 25 ± 2 s (Figures 5B and 5C). In contrast, the NEECK mutant was dramatically slower, with $t_{1/2}$ >6,134 s. The PIP2 mutant showed reduced dynamics, with $t_{1/2}$ 35 ± 4 s (Figure 5B). The slower dynamics of α-actinin-2 mutants compared to WT observed in cellula seems not to be due to F-actin binding activity, because both mutants bind F-actin (Figure 5A). Analysis of FRAP kinetics revealed standard fast and slow components in the case of WT and the PIP2 mutant, whereas for NEECK only a slow component could be discriminated. The slow, single-exponential exchange of NEECK agrees with a dominant, high-affinity interaction. Because the NEECK interaction with titin is constitutive, the slow cellular dynamics likely reflect the high affinity of the EF3-4 interaction. Exchange of the PIP2 mutant was also slower, in agreement with reduced phospholipid regulation. To probe the role of PIP2 in regulating α-actinin dynamics independently, we used the aminoglycoside neomycin, an inhibitor of PIP2 signaling (Li and Russell, 2013; Schacht, 1976). Neomycin resulted in slower FRAP recovery of WT α-actinin-2 (≈40 ± 4 s), similar to the PIP2 mutant (Figure 5C), supporting the notion that α-actinin-2 Z-disk dynamics are strongly dependent on PIP2 regulation, in agreement with the Z-disk localization of PIP2 (Figure S6A).

Z-disk morphology in α-actinin-transfected NRCs showed a striking phenotype for the NEECK mutant but not WT or the PIP2 mutant. Cells expressing NEECK showed gradual appearance of sarcomeres with wide α-actinin labeling, where titin epitopes peripheral (T12 antibody) and more central (Z1Z2) to the Z-disk (Young et al., 1998) were resolved as doublets flanking the edge of the α-actinin-labeled central Z-disk. This resulted in formation of actin/α-actinin bundles resembling nemaline rods but containing diffusely localized Z-disk titin (Figures 6A–6C) and ultimately complete disruption of sarcomeres (Figure 6C). Vinculin localization in NEECK-transfected cardiomyocytes was unaffected (Figure S6B).

Whereas the optically resolvable distance between T12 epitopes in WT-transfected cells is ∼200 nm, in NEECK-transfected cells this was >600 nm, and >800 nm after 3 days (Figure S6C). Similar splitting to >200 nm was also seen for Z1Z2, normally at the limit of optical resolution with a separation of ∼100 nm (Young et al., 1998). This suggests that the ordered integration of titin and α-actinin is severely disrupted by NEECK, raising the question of whether the spatiotemporal integration of other titin Z-disk ligands is affected. Current models of titin layout in the Z-disk predict that Z-disk widening could only be achieved by relative slipping of the overlapping N termini of titin molecules entering the Z-disk from two antiparallel sarcomere halves (Gautel, 2011). Titin molecules are crosslinked in an antiparallel palindromic complex of domains Z1-Z2 and the small Z-disk protein telethonin (Zou et al., 2006). Both telethonin and titin-Z1Z2 epitopes strictly colocalize at the Z-disk periphery (Figure 6D) but also in the wide NEECK Z-disks (Figure 6E). These results show that intramolecular autoregulation of α-actinin-ligand interactions is crucial for sarcomere integrity regulating the integration of titin, actin, and α-actinin in Z-disks of controlled width, without affecting interaction of titin with Z-disk proteins such as telethonin.

DISCUSSION

The structure of α-actinin-2 shows a modular architecture, yet is more than just "the sum of its parts": important intra- and intermolecular contacts lock the molecule in a closed conformation that is crucial for dynamic regulation.

Pseudoligand Model Validation

The structure of α-actinin-2 displays a closed, autoinhibited conformation, as suggested by Young and Gautel (2000) (Figure 1B). The closed structure of α-actinin-2 shows, furthermore, that the PIP2 binding site on the ABD (Franzot et al., 2005) maps at a suitable position and distance from the CAMD-neck interaction for sensing the hydrophobic tail of PIP2 (Figure 2A), as supported by MD/docking simulations (Figure 2G; Figures S2C–S2F).

The closed α-actinin-2 conformation shows that a number of interactions between SR1–4 stabilize the formation of antiparallel dimers, providing its structural rigidity and stability. Although addition of PIP2-C16* alone does not promote complete opening of α-actinin-2, at least as measurable by DEER, it promotes binding of Zr-7 with nanomolar affinity (Figure 3F), suggesting a positive allosteric modulation for opening and ligand binding. Furthermore, local structural changes in the CH2 domain, as observed upon PIP2 binding to nonmuscle α-actinin (Full et al., 2007), cannot be excluded.

Additional mechanisms might act in cells that cooperate with PIP2 or offer alternative regulation, including posttranslational modifications or protein cofactors. However, we could not identify any such plausible sites conserved between muscle α-actinin-2 and -3 in proteomic databases. No protein cofactors regulating α-actinin-titin interactions have been identified to date.

Structural comparison of interactions between EF3-4, Zr-7, and the neck reveals the basis for the higher affinity of α-actinin-2 for titin versus the pseudoligand neck (Young and Gautel, 2000) (Figure 2F). Our results suggest a model for PIP2 regulation of α-actinin, relying on structural plasticity and conformational dynamics of α-actinin-2 (Figure 7A): in the absence of PIP2, α-actinin-2 exists in two conformational states, a highly populated closed [A_C] and a low populated open and active state [A_O]. Addition of PIP2 triggers an activated state [A*:PIP2] with lower activation energy for opening. Binding of Zr-7 recruits α-actinin-2 in the open conformation [A_O:Zr-7], which is enriched, because α-actinin-2 binds Zr-7 with higher affinity than it does to the pseudoligand neck (Figure 2F; Table S4).

Implications for Binding F-Actin Crosslinking and Z-Disk Structure

In the Z-disk, antiparallel actin filaments are crosslinked by α-actinin in a paracrystalline tetragonal lattice (Goldstein et al., 1988). To analyze the structural determinants of α-actinin's principal crosslinking function, we mapped the known actin binding sites (ABSs) to the structure of the α-actinin dimer. ABSs in ABDs of several actin-binding proteins have been located on the first and the last α helix of the CH1 domain and on the first α helix of the CH2 domain (Sjöblom et al., 2008). ABSs in α-actinin-2 are exposed, and not blocked by interdomain interactions (Figure 7B).

To generate a 3D model of F-actin/α-actinin, we superimposed the structure of α-actinin-2 on that of the F-actin-bound

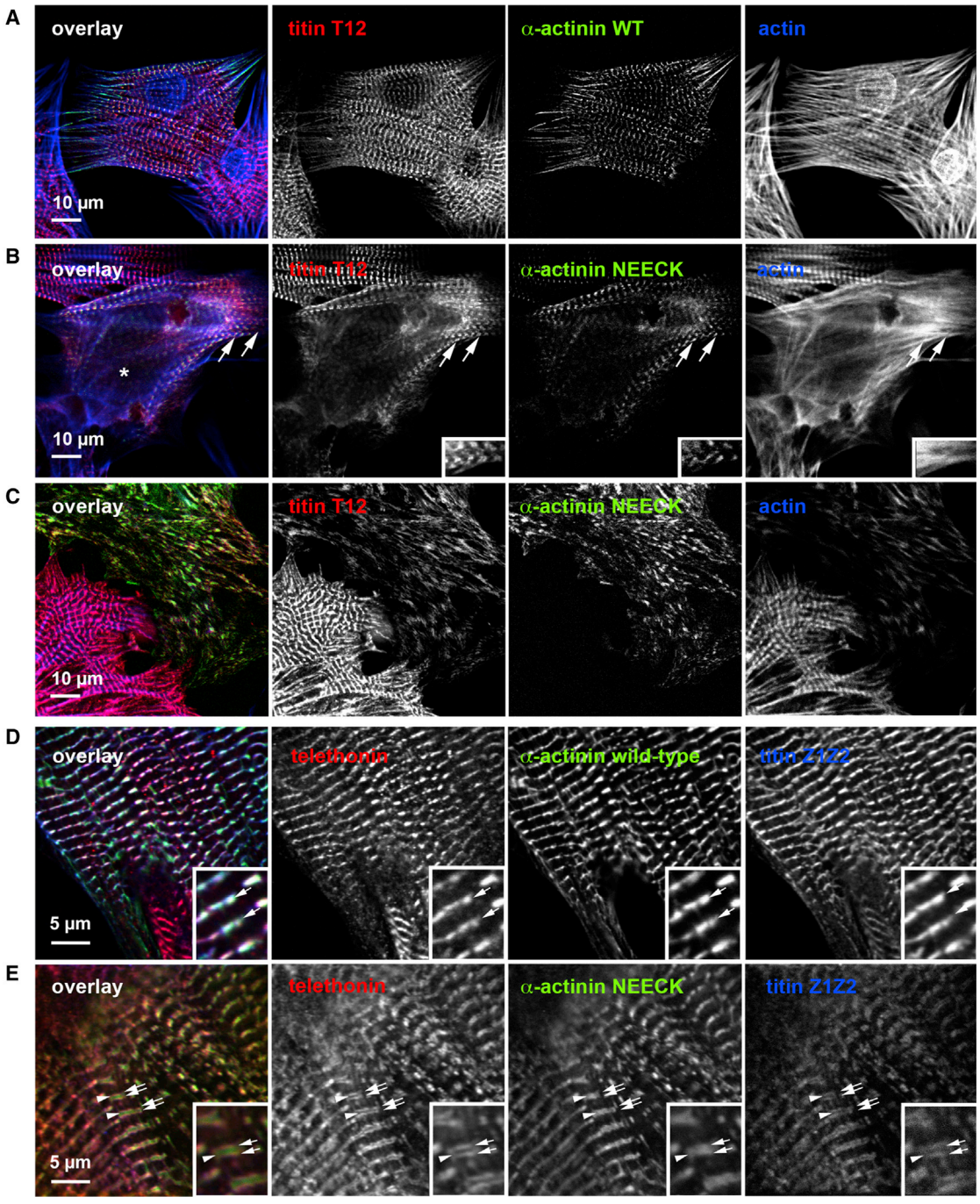

Figure 6. Constitutively Activated α-Actinin-2 Disrupts Z-Disks and Leads to Myofibril Disassembly

GFP-labeled WT and NEECK α-actinin-2 were transiently expressed in NRCs for 18–48 hr.

(A) WT α-actinin shows normal Z-disk localization, and the titin T12 epitope is resolved as a single line in standard confocal microscopy.

(B) In contrast, NEECK leads to widening of the Z-disk and splitting of the T12 epitope after ~18 hr (asterisk); doublet T12 lines are highlighted by arrows.

(C) After 48 hr, Z-disks are completely disrupted and Z-disk titin, actin, and mutant α-actinin are localized in rod-like structures.

(D and E) Superresolution microscopy reveals that epitopes of N-terminal Z1Z2 of titin and their ligand telethonin are unresolvable in WT-transfected cells; NEECK causes widening of Z-disks. Doublet Z1Z2/telethonin lines are highlighted by arrows and the central α-actinin region is indicated by arrowheads. Insets show 2-fold enlargement. Z-disk titin (T12 epitope) or telethonin, red; mutant α-actinin-GFP, green; actin (Alexa 688-phalloidin) or titin Z1Z2, blue.

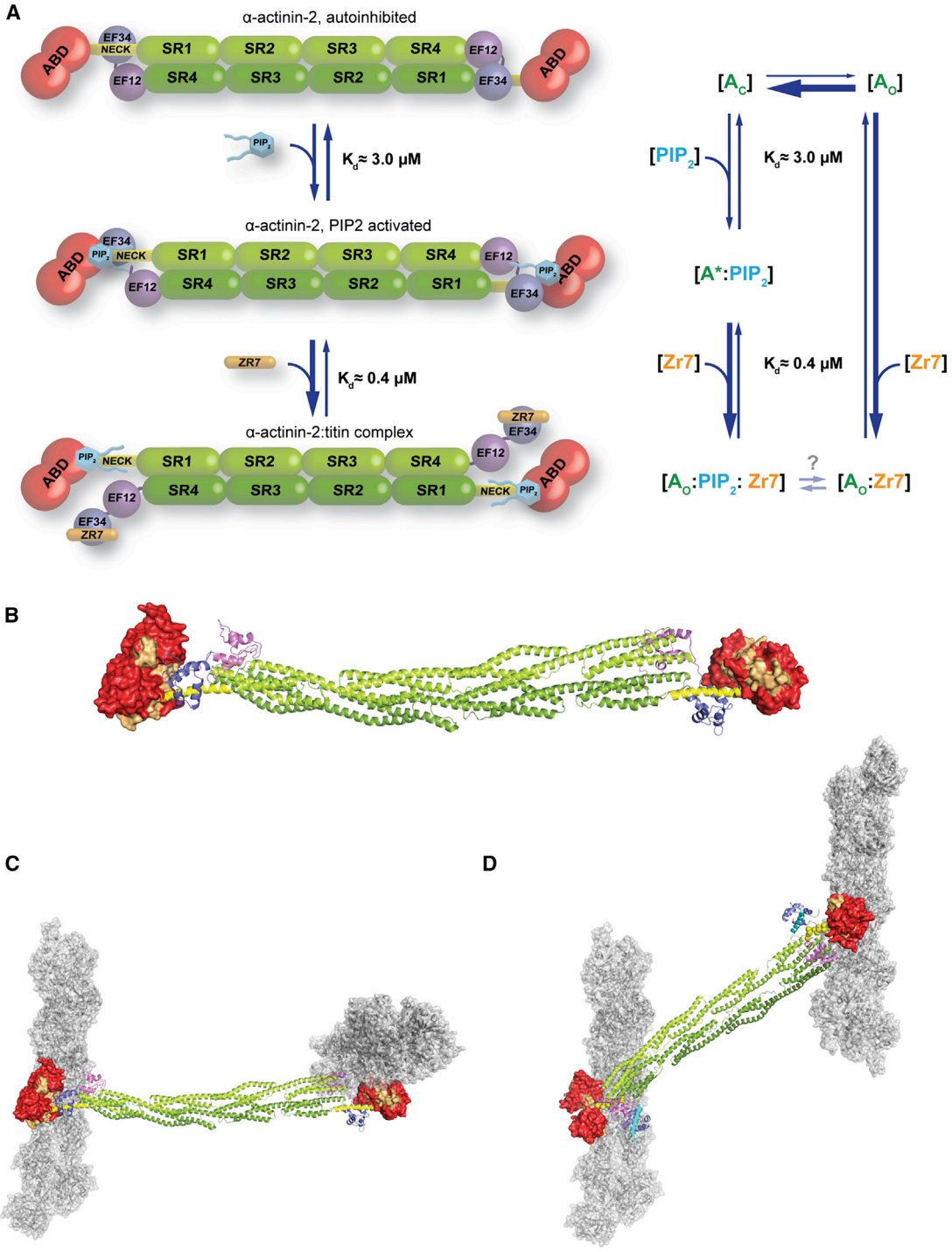

Figure 7. Molecular Mechanism of α-Actinin-2 Phosphoinositide-Based Activation and Model for F-Actin/α-Actinin Crosslinking in the Z-Disk

(A) Reaction mechanism depicting α-actinin activation by PIP2. α-actinin in the absence of PIP2 is in equilibrium between highly populated closed [A_C] and low populated open states [A_O]. Addition of PIP2 generates an activated state [A*:PIP2], with lower activation energy for opening. Binding of Zr-7 recruits α-actinin to the open conformation, leading to an increase of [A_O:Zr-7] due to higher α-actinin affinity for Zr-7 compared to the neck.

(B) Actin binding sites 1–3 (orange) mapped onto the molecular surface of ABD in α-actinin-2 in closed conformation. Color coding of domains is as in Figure 1.

(C) α-actinin-2 crystal structure superimposed on F-actin decorated by the CH1 domain of α-actinin-2 (PDB ID code 3LUE).

(D) Model of α-actinin-2 crosslinking antiparallel actin filaments. α-actinin-2 in open conformation (NEECK) was modeled assuming structural plasticity in the flexible neck, which allows for suitable orientation of ABDs. Titin Zr-7 is in cartoon presentation (cyan).

See also Movie S1.

CH1 domain (PDB ID code 3LUE) (Galkin et al., 2010). Notably, using the α-actinin-2 structure leads to a model with perpendicular actin filaments (Figure 7C), in strong disagreement with the established antiparallel actin architecture in the Z-disk but agreeing with the α-actinin-2 dimer architecture. Due to the internal twist of about 90° of the central rod (Ylänne et al., 2001), the ABDs in the dimer are rotated by 90°. We next used the structure of the NEECK mutant as the "open" structure in the Z-disk. Here the unbound neck is unstructured (Figure S4), allowing the ABD to explore different orientations, adopting those compatible with interaction with antiparallel actin filaments. Considering the angular distribution of F-actin and α-actinin, which centers at 60° and 120°, respectively (Hampton et al., 2007), we generated a model of two actin filaments crosslinked by an α-actinin-2 dimer (Figure 7D; Movie S1). In this model, the distance between filaments is ~230 Å, which is in excellent agreement with the observed interfilament distances in the tetragonal Z-disk lattice (240 Å; Goldstein et al., 1979).

The structural plasticity of α-actinin-2 has implications for not only its regulation but also for actin filament binding both in muscle and nonmuscle isoforms, where actin filaments are randomly oriented, requiring ABDs to adopt variable orientations. Interestingly, muscle α-actinin-2 was found to crosslink antiparallel as well as parallel actin filaments in α-actinin-F-actin rafts (Hampton et al., 2007). Assuming the absence of PIP2 in these assays, the flexibility of the ABD likely resides in the hinge region between the ABD and the neck (residue G258) (Figure 2A), similar to the solution structure of closed α-actinin-2 (Figure 4D). Other electron microscopy studies showed that ABDs in smooth muscle α-actinin can attain different orientations through movement in the flexible neck (Taylor and Taylor, 1993; Winkler et al., 1997), crosslinking both antiparallel and parallel actin filaments in vitro and in vivo (Meyer and Aebi, 1990; Tang et al., 2001).

Although alternative paths of titin in the Z-disk are conceivable, our results with NEECK show that even in strongly split Z-disks the Z1Z2 and telethonin epitopes remain in strict colocalization, implying that the two titin molecules crosslinked in the titin-telethonin complex must come from the same half-sarcomere, as suggested previously (Zou et al., 2006). Intriguingly, these findings also suggest that titin capping (via telethonin) and barbed-end actin filament capping by CapZ are not directly correlated, despite the close association of the titin Z1Z2-telethonin complex with the actin barbed end (Zou et al., 2006). However, actin capping by CapZ and crosslinking by α-actinin may crosstalk, as indeed α-actinin was reported to interact with CapZ via a binding site on the rod (Papa et al., 1999) and both proteins are PIP2 regulated (Figure S6A).

Impact of Pathogenic Mutations

Genetic variants in α-actinin genes are associated with several inherited diseases. Missense variants in nonmuscle actinin 1 (*ACTN1* gene) cause autosomal-dominant congenital macrothrombocytopenia (Guéguen et al., 2013; Kunishima et al., 2013), and approximately 4% of autosomal-dominant familial focal segmental glomerulosclerosis has been linked to nonmuscle *ACTN4* mutations (Kaplan et al., 2000). Missense variants in muscle *ACTN2* have been reported in sporadic cases and a few families with dilated or hypertrophic cardiomyopathy (Chiu et al., 2010; Mohapatra et al., 2003; Theis et al., 2006). Our structure now provides a platform for the analysis of mutational impact on structure, ligand binding, and regulation of α-actinin in inherited human diseases (see Supplemental Information and Figure S7).

Structural Analysis of Selected Genetic Variants

The genetic variants are spread over all domains of α-actinin. Several variants are conservative and would not lead to major structural perturbations, in particular mutations in the CAMD and the rod domain. Changes of rod surface properties might, however, abrogate interactions with ligands, because the rod domain is recognized as the prominent protein interaction platform of α-actinin (Djinovic-Carugo et al., 2002). Interestingly, the mutations on the rod domain map on the less conserved, acidic side of the convex surface (Ylänne et al., 2001) (Figure S7). However, four mutations in the *ACTN1* and *ACTN4* genes have predicted disruptive potential: E225K (*ACTN1* gene, ABD) leads to a loss of a salt bridge and mutation R738W (*ACTN1* gene, CAMD) would disrupt the structure of the CAMD, whereas the W59R (*ACTN4* gene, ABD) and S262F (*ACTN4* gene, ABD) mutations destabilize the domain structure due to introduction of charged or bulky hydrophobic residues to the core of the ABD. Most hypertrophic cardiomyopathy and dilated cardiomyopathy variants were classified as structurally neutral.

Implication for Regulation of the α-Actinin Family in General

Muscle α-actinin interacts with many proteins via multiple binding sites. The CAMD EF3-4 site interacts with helical motifs in the actin- and α-actinin-binding proteins myopalladin, palladin, and myotilin, highly similar to the α-actinin-titin complex and the intramolecular neck complex detailed here (Beck et al., 2011). Dynamic regulation of α-actinin interactions with these proteins is therefore likely governed by the same principles as the one with titin. Additionally, the α-actinin-associated LIM protein (ALP) and ZASP/Cypher bind α-actinin at both the CAMD (via its PDZ domain) and the SR (Faulkner et al., 1999; Klaavuniemi et al., 2004). Although the binding sites for titin Zr-7 and the PDZ domain on CAMD do not coincide, an open structure might be required to accommodate both binding partners and prevent steric hindrance by the spatially close α-actinin domains.

Furthermore, interactions of CAMDs of the structurally related cytoskeletal actin-binding proteins dystrophin, utrophin, and spectrin may play important roles in regulating cytoskeletal interactions near the plasma membrane (Bennett and Healy, 2008), as suggested by recent studies on spectrin-ankyrin, actin, and protein 4.2 interactions (Korsgren and Lux, 2010; Korsgren et al., 2010). Although these EF hand domains retain aspects of calcium regulation (only the N-terminal EF hand binds calcium), the general mode of regulation seems highly similar to α-actinin, namely the CH2-R1 linker region of α/β-spectrin also binds to the CAMD EF3-4 hands, and this regulates protein interactions.

The mechanism we have detailed here is therefore likely to be of general relevance for regulating spectrin-like proteins via intramolecular pseudoligand interactions.

EXPERIMENTAL PROCEDURES

Purification and Crystallization

Proteins were expressed as His fusions in *Escherichia coli* and purified via Ni-NTA agarose and size-exclusion chromatography. Protein was lysine methylated and crystallized in a precipitant containing 0.2 M Mg formate, 5% PEG smear, and 10 mM EDTA by hanging-drop vapor diffusion at 14°C.

Structure Determination

A 3.5 Å data set was collected at beamline ID23-2 (European Synchrotron Radiation Facility [ESRF]). The phase problem was solved by molecular replacement using structures of the rod domain (PDB ID code 1HCI), the ABD from α-actinin-3 (PDB ID code 1WKU), and the NMR structure of EF3-4 (PDB ID code 1H8B) as search models.

Residues 34–892 were assigned in the final model. Details on data collection, processing, structure determination, and refinement are described in Extended Experimental Procedures and Table S1.

Electron Paramagnetic Resonance

Site-directed spin labeling (SDSL) was performed on native cysteine residues of WT and NEECK α-actinin-2. X band cw EPR experiments were carried out at 298 K or 160 K on a Bruker EMX spectrometer. Pulsed EPR measurements were carried out at 50 K on a Q band power upgraded Bruker ELEXSYS E580 spectrometer. Details are given in Extended Experimental Procedures.

SAXS Measurements and Modeling

Small-angle X-ray scattering data were collected at beamline X33 at European Molecular Biology Laboratory (EMBL) Hamburg for WT, NEECK, and PIP2 mutants at three different concentrations and analyzed following standard procedures. Molecular dynamics simulations were carried out using the GROMACS 4.0.7 package (Hess et al., 2008), whereas flexible docking was performed using GOLD version 5.2.2 (Jones et al., 1997). Further details are described in Extended Experimental Procedures.

Cell Biophysics

Experiments in neonatal rat cardiomyocytes were performed using published methods and antibodies using live-cell imaging on a Zeiss LSM510 confocal microscope and superresolution on a Leica TCS STED instrument (see Extended Experimental Procedures).

ACCESSION NUMBERS

The coordinates and structure factors of the α-actinin-2 structure have been deposited in the Protein Data Bank under ID code 4D1E.

SUPPLEMENTAL INFORMATION

Supplemental Information includes Extended Experimental Procedures, seven figures, five tables, and one movie and can be found with this article online at http://dx.doi.org/10.1016/j.cell.2014.10.056.

AUTHOR CONTRIBUTIONS

Experiments were designed by M.G., K.D.-C., and E.d.A.R. in consultation with K.F.P., E.B., and D.I.S.; all structural work was performed by E.d.A.R., N.P., A.S., B.S., K.F.P., and P.V.K.; E.d.A.R., A.G., and J.K. performed biochemical work; A.G. and M.R.H. performed cell biophysics, and F.L.A. performed the NMR work; C.S. and E.A.G. assisted with protein purification and crystallization; A.A.P. and B.Ž. performed MD; and M.G., K.D.-C., E.d.A.R., and N.P. wrote the manuscript, with all authors contributing to editing the manuscript and supporting the conclusions.

ACKNOWLEDGMENTS

We are greatly indebted to Ay Lin Kho for NRC preparations. Thanks also to Dusan Turk (Institute Jozef Stefan, Ljubljana) for initial help with refinement and Oliviero Carugo (University of Vienna and University of Pavia) and Bettina Hartlieb (Baxter Innovations GmbH) for critical reading of the manuscript. We thank the staff of the MX beamlines at the ESRF in Grenoble, SAXS beamline X33 (Deutsches Elektronen-Synchrotron, Hamburg), and SWING beamline (Soleil, Saint-Aubin) for their excellent support. We thank the staff of Campus Science Support Facilities GmbH (Campus Vienna Biocenter) for technical assistance. The K.D.-C. group was supported by Austrian Science Fund (FWF) Projects I525, I1593, P22276, and P19060, by the Federal Ministry of Economy, Family and Youth through the initiative "Laura Bassi Centres of Expertise" funding the Center of Optimized Structural Studies (253275), by the Marie Curie Initial Training Network: MUZIC (238423), and by the University of Vienna. This research was also funded by the European Community Seventh Framework Programme (FP7/2007-2013) under BioStruct-X (283570). F.L.A. thanks BioTek2021 Project 217708/O10 and the Research Council of Norway for financial support. B.Ž. and A.A.P. were supported by the European Research Council (279408). A.A.P. was supported by the Russian Scientific Foundation (14-24-00118). M.G. and A.G. were supported by the Leducq Foundation Transatlantic Network of Excellence: Proteotoxicity (11 CVD 04) and the Medical Research Council of Great Britain (MR/J010456/1). A.G. and E.d.A.R. were also supported by the Marie Curie Initial Training Network: MUZIC (238423). M.G. holds the British Heart Foundation Chair of Molecular Cardiology (CH/08/001). D.I.S. acknowledges support from the Human Frontier Science Program (RGP0017/2012).

Received: May 7, 2014
Revised: October 1, 2014
Accepted: October 24, 2014
Published: November 26, 2014

REFERENCES

Atkinson, R.A., Joseph, C., Kelly, G., Muskett, F.W., Frenkiel, T.A., Nietlispach, D., and Pastore, A. (2001). Ca^{2+}-independent binding of an EF-hand domain to a novel motif in the α-actinin-titin complex. Nat. Struct. Biol. *8*, 853–857.

Bayley, P.M., Findlay, W.A., and Martin, S.R. (1996). Target recognition by calmodulin: dissecting the kinetics and affinity of interaction using short peptide sequences. Protein Sci. *5*, 1215–1228.

Beck, M.R., Otey, C.A., and Campbell, S.L. (2011). Structural characterization of the interactions between palladin and α-actinin. J. Mol. Biol. *413*, 712–725.

Bennett, V., and Healy, J. (2008). Organizing the fluid membrane bilayer: diseases linked to spectrin and ankyrin. Trends Mol. Med. *14*, 28–36.

Bernadó, P., Mylonas, E., Petoukhov, M.V., Blackledge, M., and Svergun, D.I. (2007). Structural characterization of flexible proteins using small-angle X-ray scattering. J. Am. Chem. Soc. *129*, 5656–5664.

Carugo, O. (2014). Wolumes - an algorithm to compute the volume of atoms and residues in proteins. arXiv, http://arxiv.org/pdf/1406.3242.pdf.

Chin, D., and Means, A.R. (2000). Calmodulin: a prototypical calcium sensor. Trends Cell Biol. *10*, 322–328.

Chiu, C., Bagnall, R.D., Ingles, J., Yeates, L., Kennerson, M., Donald, J.A., Jormakka, M., Lind, J.M., and Semsarian, C. (2010). Mutations in α-actinin-2 cause hypertrophic cardiomyopathy: a genome-wide analysis. J. Am. Coll. Cardiol. *55*, 1127–1135.

Djinovic-Carugo, K., Gautel, M., Ylänne, J., and Young, P. (2002). The spectrin repeat: a structural platform for cytoskeletal protein assemblies. FEBS Lett. *513*, 119–123.

Faulkner, G., Pallavicini, A., Formentin, E., Comelli, A., Ievolella, C., Trevisan, S., Bortoletto, G., Scannapieco, P., Salamon, M., Mouly, V., et al. (1999). ZASP: a new Z-band alternatively spliced PDZ-motif protein. J. Cell Biol. *146*, 465–475.

Foley, K.S., and Young, P.W. (2014). The non-muscle functions of actinins: an update. Biochem. J. *459*, 1–13.

Fraley, T.S., Tran, T.C., Corgan, A.M., Nash, C.A., Hao, J., Critchley, D.R., and Greenwood, J.A. (2003). Phosphoinositide binding inhibits α-actinin bundling activity. J. Biol. Chem. *278*, 24039–24045.

Franzot, G., Sjöblom, B., Gautel, M., and Djinović Carugo, K. (2005). The crystal structure of the actin binding domain from α-actinin in its closed conformation: structural insight into phospholipid regulation of α-actinin. J. Mol. Biol. *348*, 151–165.

Fukami, K., Furuhashi, K., Inagaki, M., Endo, T., Hatano, S., and Takenawa, T. (1992). Requirement of phosphatidylinositol 4,5-bisphosphate for α-actinin function. Nature *359*, 150–152.

Fukami, K., Sawada, N., Endo, T., and Takenawa, T. (1996). Identification of a phosphatidylinositol 4,5-bisphosphate-binding site in chicken skeletal muscle α-actinin. J. Biol. Chem. *271*, 2646–2650.

Full, S.J., Deinzer, M.L., Ho, P.S., and Greenwood, J.A. (2007). Phosphoinositide binding regulates α-actinin CH2 domain structure: analysis by hydrogen/deuterium exchange mass spectrometry. Protein Sci. *16*, 2597–2604.

Galkin, V.E., Orlova, A., Salmazo, A., Djinović-Carugo, K., and Egelman, E.H. (2010). Opening of tandem calponin homology domains regulates their affinity for F-actin. Nat. Struct. Mol. Biol. *17*, 614–616.

Gautel, M. (2011). The sarcomeric cytoskeleton: who picks up the strain? Curr. Opin. Cell Biol. *23*, 39–46.

Gautel, M., Goulding, D., Bullard, B., Weber, K., and Fürst, D.O. (1996). The central Z-disk region of titin is assembled from a novel repeat in variable copy numbers. J. Cell Sci. *109*, 2747–2754.

Goldstein, M.A., Schroeter, J.P., and Sass, R.L. (1979). The Z lattice in canine cardiac muscle. J. Cell Biol. *83*, 187–204.

Goldstein, M.A., Michael, L.H., Schroeter, J.P., and Sass, R.L. (1988). Structural states in the Z band of skeletal muscle correlate with states of active and passive tension. J. Gen. Physiol. *92*, 113–119.

Guéguen, P., Rouault, K., Chen, J.M., Raguénès, O., Fichou, Y., Hardy, E., Gobin, E., Pan-Petesch, B., Kerbiriou, M., Trouvé, P., et al. (2013). A missense mutation in the α-actinin 1 gene (ACTN1) is the cause of autosomal dominant macrothrombocytopenia in a large French family. PLoS ONE *8*, e74728.

Hampton, C.M., Taylor, D.W., and Taylor, K.A. (2007). Novel structures for α-actinin:F-actin interactions and their implications for actin-membrane attachment and tension sensing in the cytoskeleton. J. Mol. Biol. *368*, 92–104.

Hess, B., Kutzner, C., van der Spoel, D., and Lindahl, E. (2008). GROMACS 4: algorithms for highly efficient, load-balanced, and scalable molecular simulation. J. Chem. Theory Comput. *4*, 435–447.

Hoeflich, K.P., and Ikura, M. (2002). Calmodulin in action: diversity in target recognition and activation mechanisms. Cell *108*, 739–742.

Jones, G., Willett, P., Glen, R.C., Leach, A.R., and Taylor, R. (1997). Development and validation of a genetic algorithm for flexible docking. J. Mol. Biol. *267*, 727–748.

Kaplan, J.M., Kim, S.H., North, K.N., Rennke, H., Correia, L.A., Tong, H.Q., Mathis, B.J., Rodríguez-Pérez, J.C., Allen, P.G., Beggs, A.H., and Pollak, M.R. (2000). Mutations in ACTN4, encoding α-actinin-4, cause familial focal segmental glomerulosclerosis. Nat. Genet. *24*, 251–256.

Klaavuniemi, T., Kelloniemi, A., and Ylänne, J. (2004). The ZASP-like motif in actinin-associated LIM protein is required for interaction with the α-actinin rod and for targeting to the muscle Z-line. J. Biol. Chem. *279*, 26402–26410.

Klein, M.G., Shi, W., Ramagopal, U., Tseng, Y., Wirtz, D., Kovar, D.R., Staiger, C.J., and Almo, S.C. (2004). Structure of the actin crosslinking core of fimbrin. Structure *12*, 999–1013.

Korsgren, C., and Lux, S.E. (2010). The carboxyterminal EF domain of erythroid α-spectrin is necessary for optimal spectrin-actin binding. Blood *116*, 2600–2607.

Korsgren, C., Peters, L.L., and Lux, S.E. (2010). Protein 4.2 binds to the carboxyl-terminal EF-hands of erythroid α-spectrin in a calcium- and calmodulin-dependent manner. J. Biol. Chem. *285*, 4757–4770.

Krissinel, E., and Henrick, K. (2007). Inference of macromolecular assemblies from crystalline state. J. Mol. Biol. *372*, 774–797.

Kunishima, S., Okuno, Y., Yoshida, K., Shiraishi, Y., Sanada, M., Muramatsu, H., Chiba, K., Tanaka, H., Miyazaki, K., Sakai, M., et al. (2013). ACTN1 mutations cause congenital macrothrombocytopenia. Am. J. Hum. Genet. *92*, 431–438.

Li, J., and Russell, B. (2013). Phosphatidylinositol 4,5-bisphosphate regulates CapZβ1 and actin dynamics in response to mechanical strain. Am. J. Physiol. Heart Circ. Physiol. *305*, H1614–H1623.

Luther, P.K. (2009). The vertebrate muscle Z-disc: sarcomere anchor for structure and signalling. J. Muscle Res. Cell Motil. *30*, 171–185.

Masaki, T., Endo, M., and Ebashi, S. (1967). Localization of 6S component of α-actinin at Z-band. J. Biochem. *62*, 630–632.

Meyer, R.K., and Aebi, U. (1990). Bundling of actin filaments by α-actinin depends on its molecular length. J. Cell Biol. *110*, 2013–2024.

Mohapatra, B., Jimenez, S., Lin, J.H., Bowles, K.R., Coveler, K.J., Marx, J.G., Chrisco, M.A., Murphy, R.T., Lurie, P.R., Schwartz, R.J., et al. (2003). Mutations in the muscle LIM protein and α-actinin-2 genes in dilated cardiomyopathy and endocardial fibroelastosis. Mol. Genet. Metab. *80*, 207–215.

Papa, I., Astier, C., Kwiatek, O., Raynaud, F., Bonnal, C., Lebart, M.C., Roustan, C., and Benyamin, Y. (1999). αactinin-CapZ, an anchoring complex for thin filaments in Z-line. J. Muscle Res. Cell Motil. *20*, 187–197.

Saad, J.S., Miller, J., Tai, J., Kim, A., Ghanam, R.H., and Summers, M.F. (2006). Structural basis for targeting HIV-1 Gag proteins to the plasma membrane for virus assembly. Proc. Natl. Acad. Sci. USA *103*, 11364–11369.

Sanger, J.M., and Sanger, J.W. (2008). The dynamic Z bands of striated muscle cells. Sci. Signal. *1*, pe37.

Schacht, J. (1976). Inhibition by neomycin of polyphosphoinositide turnover in subcellular fractions of guinea-pig cerebral cortex in vitro. J. Neurochem. *27*, 1119–1124.

Sjöblom, B., Salmazo, A., and Djinović-Carugo, K. (2008). α-actinin structure and regulation. Cell. Mol. Life Sci. *65*, 2688–2701.

Sorimachi, H., Freiburg, A., Kolmerer, B., Ishiura, S., Stier, G., Gregorio, C.C., Labeit, D., Linke, W.A., Suzuki, K., and Labeit, S. (1997). Tissue-specific expression and α-actinin binding properties of the Z-disc titin: implications for the nature of vertebrate Z-discs. J. Mol. Biol. *270*, 688–695.

Swindells, M.B., and Ikura, M. (1996). Pre-formation of the semi-open conformation by the apo-calmodulin C-terminal domain and implications for binding IQ-motifs. Nat. Struct. Biol. *3*, 501–504.

Takeda, S., Yamashita, A., Maeda, K., and Maéda, Y. (2003). Structure of the core domain of human cardiac troponin in the Ca(2+)-saturated form. Nature *424*, 35–41.

Tang, J., Taylor, D.W., and Taylor, K.A. (2001). The three-dimensional structure of α-actinin obtained by cryoelectron microscopy suggests a model for Ca(2+)-dependent actin binding. J. Mol. Biol. *310*, 845–858.

Taylor, K.A., and Taylor, D.W. (1993). Projection image of smooth muscle α-actinin from two-dimensional crystals formed on positively charged lipid layers. J. Mol. Biol. *230*, 196–205.

Theis, J.L., Bos, J.M., Bartleson, V.B., Will, M.L., Binder, J., Vatta, M., Towbin, J.A., Gersh, B.J., Ommen, S.R., and Ackerman, M.J. (2006). Echocardiographic-determined septal morphology in Z-disc hypertrophic cardiomyopathy. Biochem. Biophys. Res. Commun. *351*, 896–902.

Tskhovrebova, L., and Trinick, J. (2010). Roles of titin in the structure and elasticity of the sarcomere. J. Biomed. Biotechnol. *2010*, 612482.

Winkler, J., Lünsdorf, H., and Jockusch, B.M. (1997). Flexibility and fine structure of smooth-muscle α-actinin. Eur. J. Biochem. *248*, 193–199.

Ylänne, J., Scheffzek, K., Young, P., and Saraste, M. (2001). Crystal structure of the α-actinin rod reveals an extensive torsional twist. Structure *9*, 597–604.

Young, P., and Gautel, M. (2000). The interaction of titin and α-actinin is controlled by a phospholipid-regulated intramolecular pseudoligand mechanism. EMBO J. *19*, 6331–6340.

Young, P., Ferguson, C., Bañuelos, S., and Gautel, M. (1998). Molecular structure of the sarcomeric Z-disk: two types of titin interactions lead to an asymmetrical sorting of α-actinin. EMBO J. *17*, 1614–1624.

Zou, P., Pinotsis, N., Lange, S., Song, Y.H., Popov, A., Mavridis, I., Mayans, O.M., Gautel, M., and Wilmanns, M. (2006). Palindromic assembly of the giant muscle protein titin in the sarcomeric Z-disk. Nature *439*, 229–233.